Comparative study of shortening and cutting strategies of single-walled and multi-walled carbon nanotubes assessed by scanning electron microscopy

Magdalena Kierkowicz[a], Elzbieta Pach[b], Ana Santidrián[c], Stefania Sandoval[a], Gil Gonçalves[a], Ester Tobías-Rossell[d], Martin Kalbáč[c]*, Belén Ballesteros[b]* and Gerard Tobias[a]*

[a]Institut de Ciència de Materials de Barcelona (ICMAB-CSIC), 08193 Bellaterra, Barcelona, Spain

[b]Catalan Institute of Nanoscience and Nanotechnology (ICN2), CSIC and The Barcelona Institute of Science and Technology, Campus UAB, Bellaterra, 08193 Barcelona, Spain

[c]J. Heyrovsky Institute of the Physical Chemistry, Dolejskova 3, 18223 Prague 8, Czech Republic

[d]Escola Universitària de Ciències de la Salut de Manresa, Universitat de Vic-Universitat Central de Catalunya, Av. Universitària 4-6, 08242 Manresa, Barcelona (Spain)

*Corresponding authors.
Tel: +34 93 5801853. E-mail: gerard.tobias@icmab.es (Gerard Tobias)
Tel: + 34 937 372 649. E-mail: belen.ballesteros@icn2.cat (Belén Ballesteros)
Tel: +420 266053804. E-mail: martin.kalbac@jh-inst.cas.cz (Martin Kalbáč)

Abstract

Short carbon nanotubes (CNTs) are desired for a variety of applications. As a consequence, several strategies have been reported to cut and shorten the length of as-produced carbon nanotubes via chemical and physical routes. The efficiency of a given strategy largely depends on the physico-chemical characteristics of the CNTs employed. In order to be able to directly compare the advantages and disadvantages of commonly used protocols, a single batch of chemical vapor deposition single-walled CNTs (SWCNTs) and a batch of multi-walled CNTs (MWCNTs) were subjected to four cutting/shortening strategies, namely acid cutting, piranha treatment, steam shortening and ball milling. The length distribution was assessed by means of scanning electron microscopy. Sample purity and CNT wall structure were determined by Raman spectroscopy, thermogravimetric analysis and magnetic measurements. Within the employed experimental conditions, piranha treatment turned out to be the most efficient to achieve short SWCNTs with a narrow length distribution in a good yield, whereas a mixture of sulfuric/nitric acid was preferred in the case of MWCNTs. A subsequent short steam treatment allowed to remove functional groups present in the samples, leading to median length distributions of 266 nm and 225 nm for SWCNTs and MWCNTs respectively after the combined protocols.

1. Introduction

Carbon nanotubes (CNTs) are important players in the emerging field of nanotechnology. Compared to other materials they show unique combination of mechanical, optical and electrical properties. Their hollow structure allows the encapsulation of a wide variety of compounds in their interior [1-3] while the modification of the external walls [4, 5] further expands their range of application from composite materials, through energy field, to drug delivery [5-9]. However, some obstacles need to be overcome in order to exploit their full potential. As-produced CNTs typically have lengths up to few tens of micrometers and exhibit strong hydrophobicity, thus limiting their processability. Short and functionalized nanotubes present a higher dispersibility and biocompatibility and are thus desired for some of the targeted applications [10, 11]. In nanomedicine, CNTs with lengths typically below ca. 300 nm not only enhance their biocompatibility but also the cellular uptake [12, 13]. Biopersistence tests, which can be an indicator of the toxicity of nanomaterials, revealed that short CNTs are cleared faster from the lungs than their long counterparts [14]. Furthermore, short and properly functionalized nanotubes present the best characteristics for undergoing an efficient biodegradation [15]. Short CNTs can self insert into the lipid bilayer when their length is comparable to the thickness of the membrane [16], and they have been recently investigated as potential biological channel platforms [17]. The shortening of CNTs also has an impact on the properties of the CNTs themselves and on hybrid materials. For instance, the use of short CNTs improves the magnetic resonance imaging properties of CNTs decorated with iron oxide nanoparticles [18]. Short CNTs exhibit excellent transport properties for gas, water, ions and DNA [19-23], making them attractive for gas separation and desalination [24, 25]. The thermal and electrical conductivity of CNTs is also length dependent. One of the requirements to achieve ballistic electron transport in these nanostructures is to decrease their dimensions. It has been reported that single-walled CNTs of ca. 10 nm show negligible electrical resistivity and can withstand high currents of up to 70 μA [26]. The processability of CNTs is also enhanced when dealing with short nanostructures. For instance, cut CNTs can be more easily integrated into polymeric matrices, which is

of interest for tuning the mechanical properties of the resulting composite materials [27]. The presence of short CNTs can also improve the permability of polymer membranes up to 40% [28].

Just from the examples mentioned above it is not suprising that several strategies have been explored to reduce the length of as-produced CNTs via chemical or physical methods. Chemical strategies are based on reactions which occur on side-wall defects (cutting) and highly reactive ends (shortening). As a result, functionalized and/or open-ended nanotubes are generally obtained. These strategies include but are not limited to acid etching [29], fluorination [30], ozonolysis [31] and steam treatment [32]. Physical routes cover different types of radiation (electrons,[33] ɣ-rays[34]), sonication [35] (applying sound energy) and mechanical cutting [36] (when shear forces are involved).

Each of the performed protocols not only has different efficiencies and yields, but might also result in samples with a variety of structural defects, functional groups and impurities. Therefore the choice of one strategy or another will largely depend on the targeted application. Since the physico-chemical properties of carbon nanomaterials are largely dependent on the source of the material (method employed for their synthesis), direct comparison between already published protocols is not possible. Therefore, comparative studies, where different cutting/shortening strategies are employed on the same batch of CNTs, are necessary in order to get further insights on the advantages and disadvantages of a given method. Here we report on a comparative investigation on commonly employed strategies to prepare samples of short carbon nanotubes. The best cutting strategies under the employed experimental conditions turned out to be piranha for single-walled CNTs (SWCNTs) and a mixture of nitric and sulfuric acids for multi-walled CNTs (MWCNTs). In both cases we suggest a subsequent short steam treatment to render samples of high quality short CNTs.

2. Experimental

2.1 *Materials*

Hydrochloric (37%) and sulfuric (98%) acids were purchased from Panreac Applichem. Nitric acid (65%) and filtration membranes (Whatman Cyclopore, PC, pore size 0.2 μm) were bought from

Fischer Scientific. Hydrogen peroxide (35 %) was purchased from Acros Organics. In this study Elicarb® chemical vapour deposition (CVD) grown SWCNTs and MWCNTs were employed (Thomas Swan Co. Ltd.). The as-received SWCNTs also contained a fraction of double-walled carbon nanotubes (DWCNTs), carbonaceous impurities and iron catalyst surrounded by graphitic shells. The outer diameter of the SWCNTs is 2.1 nm and MWCNTs is 10-12 nm (values provided by the supplier). Two additional samples were prepared using arc-discharged MWCNTs. The MWCNTs were collected from as produced cathod deposit (>7.5 % MWCNTs basis, Sigma-Aldrich). The outer diameter of the arc-discharged MWCNTs is 7-15 nm (value provided by the supplier).

2.2 *Employed protocols*

2.2.1 *Steam treatment*

CNTs (400 mg) were finely ground in an agate mortar with a pestle, and then were loaded into a silica tube and placed in the center of an alumina tube in a tubular furnace. The whole system was purged with argon for 2 h to allow the complete removal of oxygen. The CNTs were treated with water steam under argon atmosphere at 900 °C for the desired amount of time (1, 12 or 25 h) and subsequently refluxed with 6 M HCl overnight. The sample was vacuum filtered onto a polycarbonate (PC) membrane, rinsed with distilled water until the pH of the filtrate was neutral and dried in the oven at 100 °C [32, 37].

2.2.2 *Acid treatment*

CNTs (300 mg) were immersed in 300 mL of a mixture of concentrated H_2SO_4/HNO_3 (vol/vol 3:1) and sonicated for 24 h at temperature between 35 °C and 40 °C as previously reported[38]. We employed a concentration of 1 mg/mL. The resulting suspension was diluted with distilled water and vacuum filtered onto a PC membrane, rinsed with distilled water until the pH of the filtrate was neutral and dried in the oven at 100 °C.

2.2.3 *Piranha reaction*

Fresh piranha solution (96% H_2SO_4/ 30% H_2O_2, vol/vol 4:1) was prepared and cooled down to room temperature in an ice bath. Then, CNTs (300 mg) were dispersed in the oxidant mixture (300 mL) and stirred with magnetic bar for 2 h.[39]. We used the same concentration of CNTs (1 mg/mL) as in

the acid treatment protocol. The reaction was quenched by dilution with distilled water and filtered onto a PC membrane. Then, it was rinsed with distilled water until the pH of the filtrate was neutral and dried in the oven overnight at 100°C.

2.2.4 *Ball milling*

This protocol was inspired by work of Rubio and coworkers,[36] but the parameters were adjusted to the capabilities of our equipment. 50 mg of CNTs were placed into a 50 mL stainless steel grinding bowl with six stainless steel balls (1 cm diameter). The setup was closed inside an Ar-filled glovebox (Labconco). Next, the container was placed in the planetary mill (Retsch PM 100 Planetary Mill) for 30 min. The rotation speed was 500 rpm and the direction of rotation was reversed each 5 min. Ball milled CNTs were subsequently refluxed with 6 M HCl overnight. The sample was filtered under vacuum onto a polycarbonate (PC) membrane, rinsed with distilled water until the pH of the filtrate was neutral and dried in the oven at 100 °C.

2.3 *Characterization*

Length distribution was determined by Scanning Electron Microscopy (SEM) on a FEI Magellan 400L XHR. The use of In-Lens Detector (TLD) at a landing energy of 2 kV enabled to obtain surface sensitive images with spatial resolution below 1 nm, allowing the visualization of individual CNTs. Acquired images were analyzed using Digital Micrograph software. 200 individual nanotubes were measured in each case. For the samples of as-received SWCNTs and steam treated SWCNTs (25 h + HCl), 200 measurements were randomly taken from the analysis performed in Ref. [37]. To perform the analysis of the rest of samples, CNTs were initially sonicated during 30-60 minutes in ortho-dichlorobenzene (Sigma Aldrich) till good dispersion was achieved. Then, so-obtained lightly grayish suspension was drop casted onto a carbon coated copper grid. Atomic Force Microscopy (AFM) images were acquired with an Agilent 5100. A tapping mode was employed using FORT tips, with a frequency of 65 kHz and a force constant of 3 N/m.

Thermogravimetric analysis (TGA) was performed with a NETZSCH-STA 449 F1 Jupiter instrument under flowing air (25 mL/min) using a ramp of 10°C/min up to 900°C. Around 5 mg of each sample were employed for each analysis.

Magnetic measurements were aquired in a Superconducting Quantum Interference Device (SQUID) magnetometer (LOT-QuantumDesign Iberia) with an applied field from −50.000 Oe to +50.000 Oe at 10 K to obtain the hysteresis loops. A diamagnetic gelatine capsule was filled with 5-8 mg of sample. The amount of iron in each of the analyzed samples was determined by taking into account the magnetic saturation of the bulk material (Ms_{Fe} = 221.7 emu·g^{-1}).

Raman spectroscopy was performed using a LabRAM HR Raman spectrometer (Horiba Jobin-Yvon), and laser excitation energies of 2.54 and 2.33 eV (488 and 532 nm, respectively, Ar/Kr laser, Coherent) and of 1.96 eV (633 nm, He-Ne). A 50x objective was used with a laser spot of about 1 μm. The laser power was 1 mW and the spectral resolution was 1 cm^{-1}. Each sample was measured in multiple regions under ambient conditions and their average was analyzed. Raman mapping was used to characterize the samples, because they were not homogeneous. Measurements were conducted with lateral steps of 1 μm (both in X and Y directions) on rectangular areas with varying sizes (49 data points or 900 data points for each map). Intensity ratios were determined from the height of the peaks.

XPS measurements were performed with a Phoibos 150 analyzer (SPECS GmbH, Berlin, Germany) in ultra-high vacuum conditions (base pressure 1E-10 mbar) with a monochromatic Kalpha x-ray source (1486.74 eV). The overall resolution for XPS, as measured by the full width at half-maximum intensity (FWHM) of the Ag 3d5/2 peak for a sputtered silver foil, is 0.57 eV.

3. Results and Discussion

Initially, the as-received SWCNTs and MWCNTs were independently treated via the following methods: steam, ball milling, a mixture of concentrated sulfuric and nitric acids (H_2SO_4/HNO_3, vol/vol 3:1), and piranha (96% H_2SO_4/ 30% H_2O_2, vol/vol 4:1). These are commonly used shortening and cutting protocols that include both chemical (steam, nitric/sulfuric and piranha) and physical methods (ball

milling). Among the chemical methods, both gas phase (water steam) and liquid phase reactions (nitric/sulfuric, piranha) are objects of the present study. After each of the treatments, CNTs were dispersed in *ortho*-dichlorobenzene and dropcasted onto a carbon coated copper grid so that individual nanotubes were obtained, and characterized by SEM. Representative images of the different samples are shown on Figure S1 (SWCNTs) and Figure S2 (MWCNTs). Just by visual inspection we can observe that as-received CNTs have lengths of several μm, which are significantly decreased after most of the employed treatments. Since AFM is the most commonly employed technique to determine the length of CNTs we initially confirmed that the length analysis by SEM would be as precise. To do so same areas of as-received SWCNTs were imaged by both techniques and one of these comparative images is included in Figure 1. The bright dots that are visible in both imaging modalities are attributed to catalytic and graphitic particles present in the as-received material. Height profiles, such as the inset in Figure 1b, were performed along several nanotubes and revealed the presence of individual CNTs. A low magnification SEM of the imaged area is included in Figure S3 where a good dispersion of CNTs can be observed. Having confirmed the suitability of SEM to determine the length of individual CNTs, the length distribution of both as-received and the treated samples was next determined by measuring 200 individual carbon nanotubes for each sample from SEM images. The performed SEM analysis can easily discern between individual CNTs, bundles and aggregates. The resulting histograms are presented in Figure 2 (SWCNTs) and Figure 3 (MWCNTs). The fraction of CNTs with lengths below 500 nm is represented in Figure S4 (SWCNTs) and Figure S5 (MWCNTs).

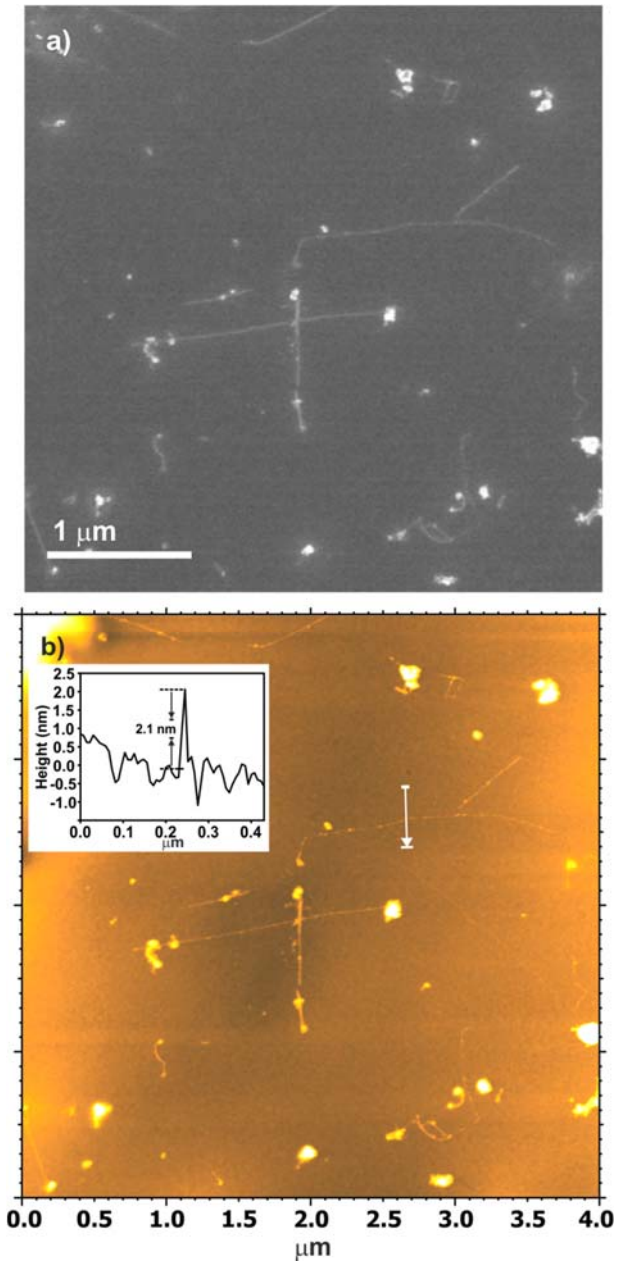

Figure 1. a) SEM and b) AFM images from the same area of as-received CVD SWCNTs deposited onto a carbon coated copper grid. The bright dots visible in both imaging modalities are attributed to catalytic and graphitic particles. Inset in (b) shows the recorded height profile along the white arrow confirming the presence of an individual SWCNT.

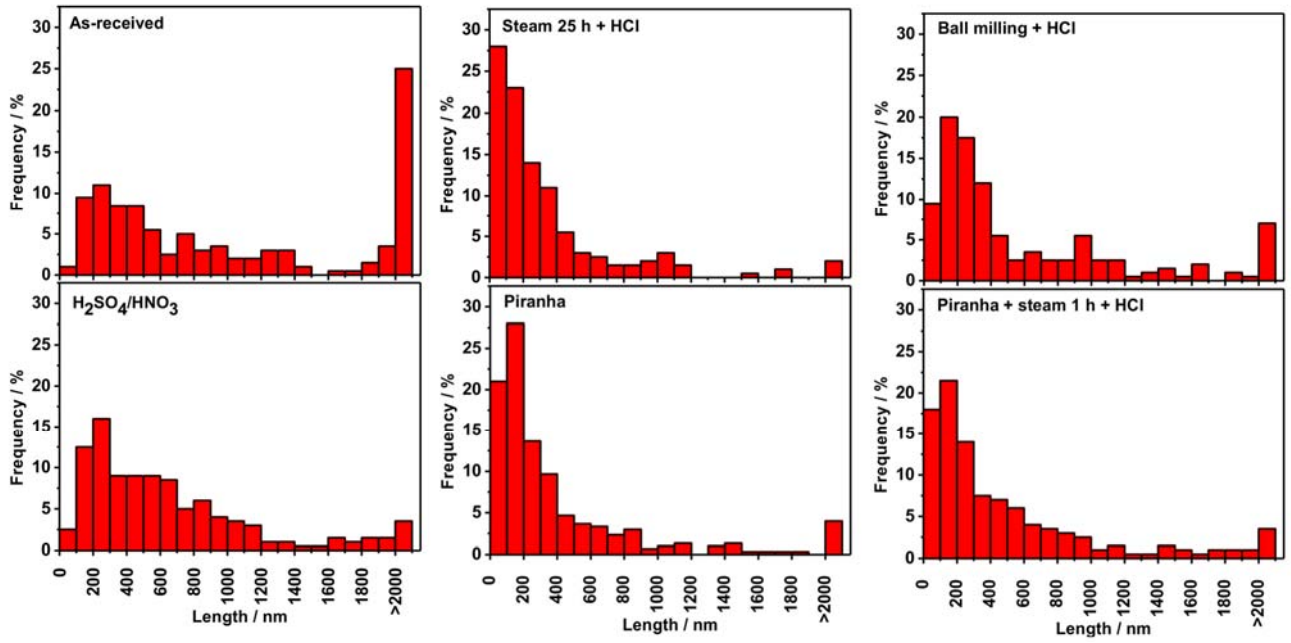

Figure 2. Length distribution histograms of as-received and treated CVD SWCNTs based on SEM image analysis.

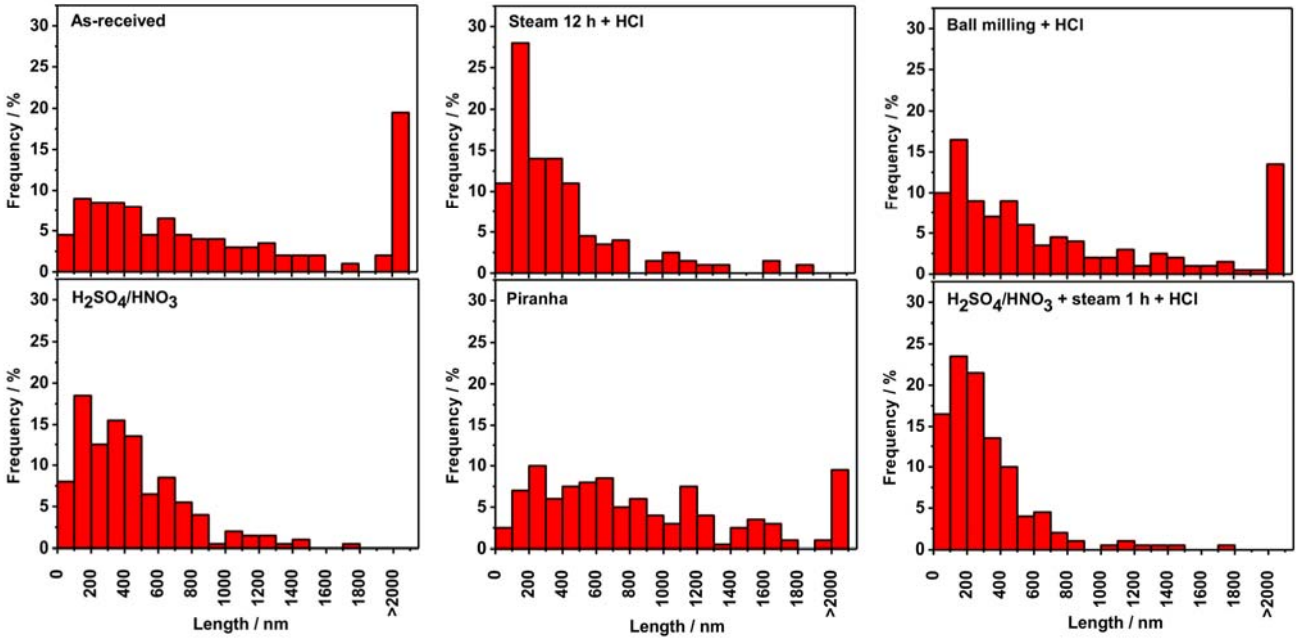

Figure 3. Length distribution histograms of as-received and treated CVD MWCNTs based on SEM image analysis.

As-received SWCNTs have a broad length distribution with a median length of 768 nm, which decreased drastically after 25 h of steam treatment to 198 nm. However, despite being very efficient in

shortening SWCNTs, this method is characterized by a low production yield, around 10 %. This is because steam preferentially reacts through the ends of SWCNTs and "eats" the SWCNTs up, therefore each long SWCNT will result in a corresponding short SWCNT. The steam shortening strategy contrasts to cutting strategies where from one individual long CNT several short CNTs can be obtained. The steam treatment goes through the following reactions [40]:

$$C_{(s)} + H_2O_{(g)} \rightarrow CO_{(g)} + H_{2\,(g)} \quad (1)$$

$$CO_{(g)} + H_2O_{(g)} \rightarrow CO_{2\,(g)} + H_{2\,(g)} \quad (2)$$

In contrast to steam, ball milling is a physical method based on shear forces. Depending on the pressure locally generated by collision of balls different morphologies can be achieved which range from cut nanotubes [36] to carbonaceous nanoparticles[41]. Therefore, to avoid structural damage of CNTs we employed a short time of milling but as it can be appreciated in the statistical analysis cutting turned out to be not so efficient. The median length of the obtained SWCNTs was 328 nm, but a high fraction of nanotubes above 2 μm was still preserved. We next investigated the liquid phase chemical strategies, namely acid and piranha cutting. Acid H_2SO_4/HNO_3 cutting led to a broader length distribution than steam with a median length of 507 nm. Finally, cutting with piranha enabled to obtain short SWCNTs (median 221 nm) with a much higher yield than the steam treatment. Our findings that piranha is more efficient in cutting SWCNTs than the mixture of H_2SO_4/HNO_3 are in agreement with the work of Liu et al. [42] despite different conditions were employed.

During the preparation of piranha the generation of Caro's acid (H_2SO_5) occurs [39]:

$H_2SO_4 + H_2O_2 \rightarrow H_2SO_5 + H_2O$ (3),

which decomposes to singlet oxygen that reacts with carbon atoms [43]:

$HSO_5^- + SO_5^{2-} \rightarrow HSO_4^- + SO_4^{2-} + {}^1O_2$ (4),

When the mixture of sulfuric and nitric acids is employed, nitronium ions are generated [44]:

$HNO_3 + 2H_2SO_4 \leftrightarrow NO_2^+ + H_3O^+ + 2HSO_4^-$ (5).

From the statistical analysis performed so far on the length distribution of SWCNTs samples, piranha arises as an appealing option when a large amount of sample is needed, because short SWCNTs are obtained in a good yield. However, the use of strong oxidants may alter the structure of CNTs and add functional groups. Since steam has been proven very efficient in removing defects and functionalities from the walls of SWCNTs [40], we next employed a combined piranha and a short steam (1 h) followed by an HCl treatment. This combined treatment resulted in a good yield (ca. 70%) of short SWCNTs (median 266 nm). Actually, the steam treatment does not introduce significant differences in the length distribution of the material. To compare both groups of SWCNTs (piranha treated with and without the 1 h steam + HCl treatment), we employed the Mann-Whitney (Wilcoxon) test because the data do not follow a normal distribution. The statistical hypothesis testing is not significant (p-value = 0.120 > 0.05), meaning that the two groups present no differences.

Before analyzing the quality of the different samples by thermogravimetric analysis (TGA) and Raman spectroscopy, let us first focus on the effect of the different treatments on the length of MWCNTs.

The median length of as-received MWCNTs was 708 nm. Steam-treated MWCNTs show a similar trend as in the case of SWCNTs where short nanotubes (median 274 nm) with a narrow length distribution were obtained. The time of steam treatment employed for MWCNTs was 12 h and in the case of SWCNTs was 25 h, because in the present case shortening occurs faster [32]. Although steam is very efficient in shortening CNTs leading to samples with a narrow length distribution, the major drawback of the steam treatment compared to the other employed protocols for cutting MWCNTs is that it presents the lowest yield of reaction. MWCNTs processed by ball milling reveal a broad length distribution with a high fraction (ca. 15%) of nanotubes above 2 μm. When it comes to liquid chemical processing of MWCNTs, whereas piranha treatment turned out to be very efficient for shortening SWCNTs, this is not the case for MWCNTs. The Mann-Whitney (Wilcoxon) test between both groups (as-received and piranha) is not significant (p-value = 0.805 > 0.05). This means that these groups present no significant differences. Therefore the length distribution of as-received MWCNTs (median

708 nm) has not been altered by the piranha treatment (median 714 nm). In contrast, short nanotubes with a median length of 365 nm were obtained by etching MWCNTs with a mixture of H_2SO_4/HNO_3 at room temperature with a narrow length distribution and a good yield. We should note that following the protocols employed in the literature, CNTs were exposed to H_2SO_4/HNO_3 for 24 h and to piranha for 2 h. Further studies would be therefore needed using both piranha and H_2SO_4/HNO_3 for different periods of time on samples of as-received SWCNTs and MWCNTs. From the different employed strategies, H_2SO_4/HNO_3 turns out to be the most attractive when it comes to cutting MWCNTs. Nevertheless, as mentioned before the use of strong oxidizing acids is known to introduce functional groups into the CNT structure[38, 45, 46]. Therefore, as in the case of SWCNTs we next performed an additional short steam treatment (1 h) followed by HCl to remove the introduced functionalities. The combined treatment resulted in a median length of 225 nm with 85% of MWCNTs below 500 nm. The yield of cutting was about 75%. We also performed the Mann-Whitney (Wilcoxon) test to compare the length distribution of both groups of MWCNTs (H_2SO_4/HNO_3 treated with and without the 1 h steam + HCl treatment). In this case, the statistical hypothesis testing revealed significant differences (p-value = $0.002 \times 10^{-2} < 0.05$). Therefore a subsequent 1h steam treatment to the MWCNTs previously cutted with H_2SO_4/HNO_3 further reduces the length distribution. The median length is decreased from 365 nm down to 225 nm.

Figure 4 displays the box plot analyses of both as-received and treated CNTs and the corresponding descriptive statistical analysis of the different samples is presented in Table S1.
Box plot analysis shows a graphical representation of the distribution of the data through their quartiles, indicating the range where most values fall and those values which differ considerably from the norm (atypical values). Regardless of the employed treatment, a non-symmetric length distribution is presented by all of the investigated samples. As-received CNTs are characterized by a broad length distribution with maximum adjacent observations of 4.4 μm (SWCNTs) and 3.2 μm (MWCNTs). A

much narrower length distribution is clearly achieved after the proposed combined treatments of piranha and sulphuric/nitric acids with steam, for SWCNTs and MWCNTs respectively.

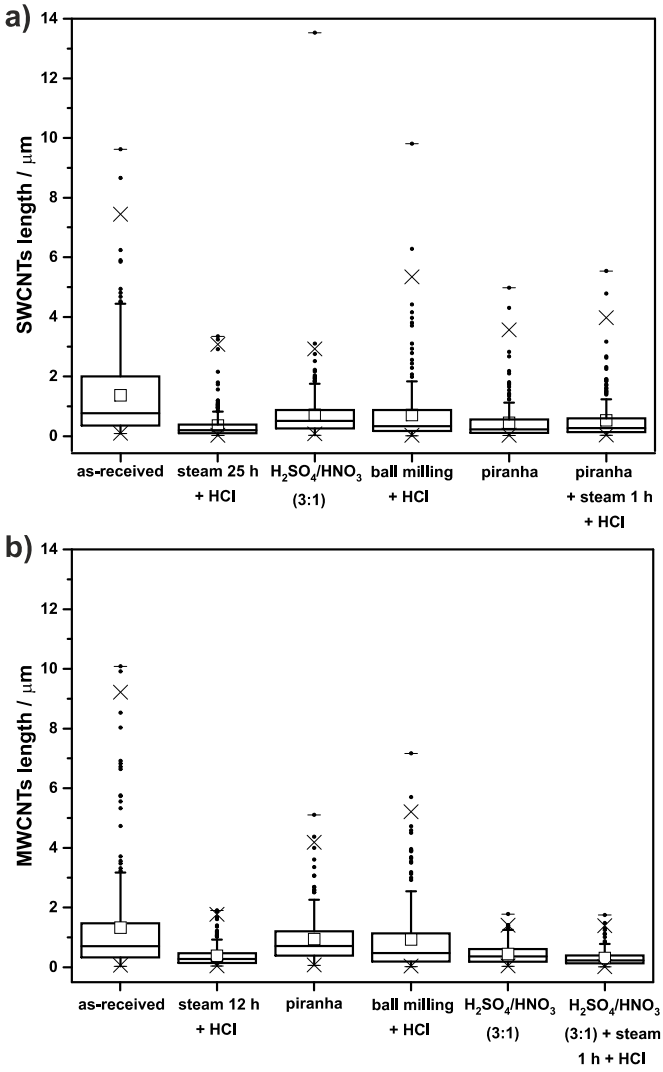

Figure 4. Box plot analysis of the as-received and treated a) CVD SWCNTs and b) CVD MWCNTs. Black dots identify outliers, empty squares mean length, cross border 99% or 1% of population, dash maximum or minimum length. The lower and maximum adjacent observations are represented with horizontal lines at the end of the whiskers.

Raman spectroscopy measurements were performed to evaluate the effect of different shortening protocols on the structure of CNTs (Figure 5). Raman spectra of CNTs present several features. Here we analyzed the tangential mode (G-band) centered at 1588 cm^{-1}, containing an axial and a circumferential

components, which can be used to distinguish between metallic and semiconducting SWCNTs by its line shape;[47, 48] additionally, for samples containing structural defects, the disorder induced mode (D-band) at lower frequencies than the G-band was observed. The D-band originates from a second-order Raman process. In this process, the incident photon resonantly excites an electron-hole pair. The electron is subsequently scattered under emission/absorption of a phonon. To satisfy the conservation of momentum, the electron has to be scattered back to a point in k-space where its momentum is near that of the initial hole. For the D mode in the Raman spectrum, the backscattering is achieved by a defect. The intensity of the D-band has been used to analyze the quality of the CNTs as it is sensitive to structural defects in the graphitic sp^2 network[49].

The D-band is the most frequently used mode for the characterization of the treated and functionalized CNTs since the relative intensity of this mode can provide evidence of covalent modification and/or defect concentration. The intensity ratio I_D/I_G is suggested to be a sensitive measure for the concentration of defects in carbon nanotubes. Figure 5 shows the D-band and the G-band spectra of CNTs excited by different laser lines: 1.96 eV (a), 2.33 eV (b) and 2.54 eV (c).

The shapes of G-bands are typical for CNT bundles where the widths of the G-band are about 20 cm^{-1} (isolated nanotubes exhibit smaller widths)[49]. The line shape of the G-band indicates that semiconducting and metallic carbon nanotubes are in resonance at the used laser excitation energies. When nanotube bundles are excited in resonance with the transition of metallic nanotubes, the G^- is broadened[50]. The D-band appears at 1347 cm^{-1} using 2.54 eV, at 1343 cm^{-1} using 2.33 eV and at 1320 cm^{-1} using 1.96 eV as excitation energy, because the frequency of the D-band is laser excitation energy dependent[51]. The intensity ratio of the D-band and the G-band (I_D/I_G ratio) reflects the defect density of CNTs. The values of I_D/I_G ratio are shown in Table 1 and plotted in Figure S6.

Table 1. Summary of the length, purity and spectroscopic properties of as-received and treated CNTs. n.d. = non-detectable.

Sample	Median length (nm)	Fraction below 500 nm (%)	Inorganic impurities (wt. %)[a)]	Iron content (wt. %)[b)]	Onset of combustion (°C) [a)]	Raman I_D/I_G ratio[c)]		
						Laser wavelength (nm)		
						633	532	488
SWCNTs								
as-received	768	39	4.6	1.43	557	1.00	1.00	1.00
steam 25 h + HCl	198	82	7.8	0.84	580	0.22	0.60	0.36
ball milling + HCl	328	65	2.4	1.42	560	1.02	0.61	1.23
H_2SO_4/HNO_3	507	49	2.5	0.60	500	0.97	2.16	1.08
Piranha	221	77	3.5	0.04	516	0.69	1.26	1.17
piranha + steam 1 h + HCl	266	68	2.2	0.91	575	0.57	0.77	0.69
MWCNTs								
as-received	708	39	3.5	1.54	576	1.00	1.00	1.00
steam 12 h + HCl	274	78	0.5	n.d.	631	1.47	1.34	1.34
ball milling + HCl	474	52	1.6	0.03	373	1.09	1.08	1.01
H_2SO_4/HNO_3	365	68	1.9	0.79	567	1.08	1.00	1.05
Piranha	714	33	3.6	1.31	535	1.05	1.03	1.02
H_2SO_4/HNO_3 + steam 1 h + HCl	225	85	1.3	0.01	633	1.50	1.46	1.30

a) based on TGA; b) based on magnetic measurements; c) spectra were normalized to I_D/I_G ratio of as-received CNT

In the case of SWCNTs, a decrease in the I_D/I_G ratio is observed after the steam treatment, regardless of the laser energy employed, which can be assigned to the removal of amorphous carbon and the SWCNTs containing a large number of defects. The I_D/I_G ratio recorded for the samples treated by ball milling, sulfuric/nitric acid and piranha is highly dependent on the laser excitation energy. The explanation for these effects may not be straightforward, because only Raman modes of tubes which are

in resonance with laser excitation energies can be found in the spectra. The resonance conditions are different for different tube diameters and also for metallic and semiconducting type of nanotubes. If the content of different electronic types or specific diameters of tubes are selectively removed by the treatment method, the Raman response would be different and also its dependence on laser excitation energy will be changed. For example piranha, as well as H_2SO_4/HNO_3, have been reported to selectively eliminate the smaller diameter nanotubes from the material[42]. Whereas a decrease in the I_D/I_G ratio is observed when the piranha treated sample is excited using 1.96 eV (633 nm), an increase in the I_D/I_G ratio is recorded upon excitation with 2.54 eV (488 nm, blue laser) or 2.33 eV (532 nm, green laser). Interestingly a decrease on the I_D/I_G ratio is achieved on this piranha treated sample after performing a 1 h steam treatment, regardless of the energy employed to record the Raman spectra. This confirms the removal of functionalities, structural defects that might have been introduced by piranha or residual amorphous carbon (which could be created by the destruction of CNTs). As expected, the sulfuric/nitric acid treatment results in an increase of the I_D/I_G ratio up to 2.16 when using the green laser. It is well established that this chemical treatment leads to structural damage of the SWCNTs. Actually, the use of strong acids can even result in the formation of carboxylated carbonaceous fragments (CCF) that will contribute to the D-band[52]. Until now it has not been possible to distinguish between the contribution to the D-band from amorphous carbon and from defects on nanotubes.

In the case of MWCNTs, the I_D/I_G ratio is not reduced with any of the employed treatments. Particularly, after the steam treatment, the I_D/I_G ratio increases significantly. This observation is in contrast to the steam treatment of SWCNTs, where a decrease of the I_D/I_G ratio is observed. In case of MWCNT only the outer wall tube is expected to be modified by the used treatment methods. As the outer tubes represent only a small fraction of the sample their contribution to the Raman spectrum is also very small. In a recent study by Baik et al. a decrease of I_D/I_G ratio is also reported on carbon nanotubes fibers after being treated with steam[53]. The steam treated nanofibers present an increase on their electrical conductivity.[53] To get further insights on the structural integrity and impurities on the CNT samples, thermogravimetric analysis (TGA) was next performed.

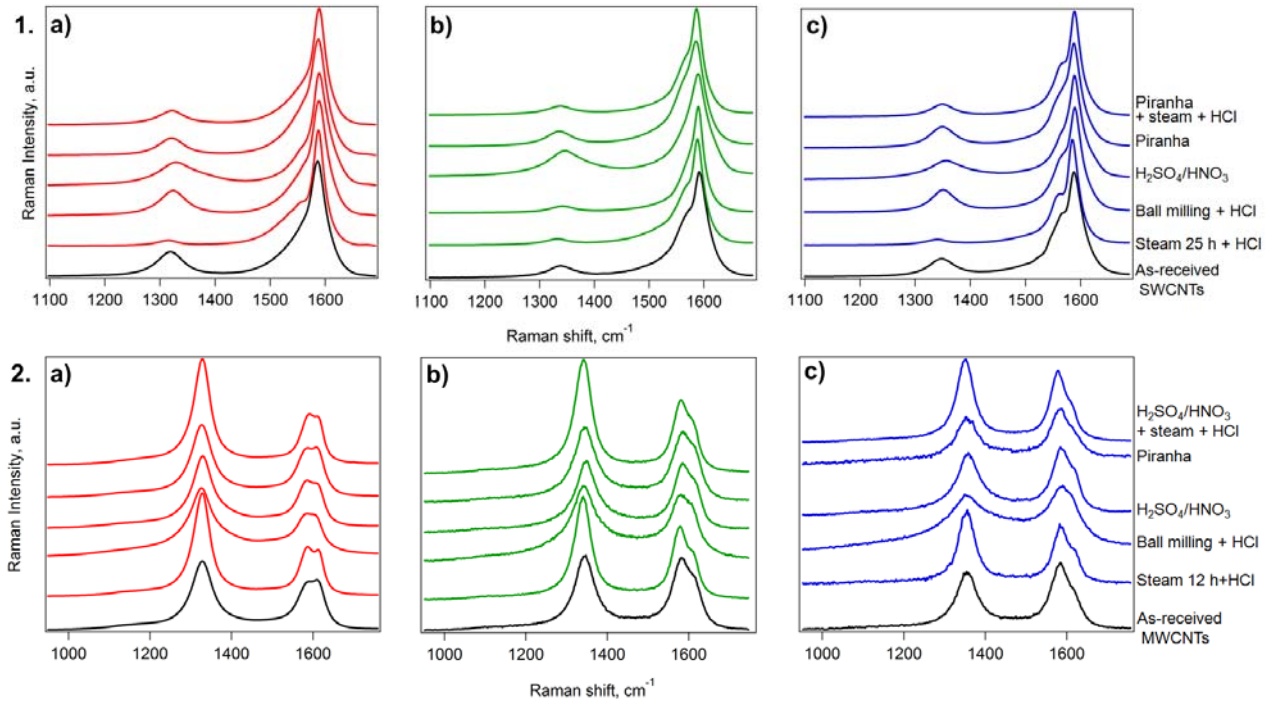

Figure 5. 1. CVD SWCNTs, 2. CVD MWCNTs. Avaraged resonance Raman spectra (D and G-band region) of as-received (black line) and treated CNTs (color lines from bottom to top: steam treatment 25 h and HCl, ball milling and HCl treatment, acid H_2SO_4/HNO_3 treatment, piranha solution treatment, combination of acid H_2SO_4/HNO_3 and steam treatment (followed by HCl)) excited by different laser lines a) 1.96 eV, b) 2.33 eV and c) 2.54 eV. Each spectrum is an average based on 900 (1.96 eV) and 49 spectra (2.33 and 2.54 eV) measured in different points. Spectra were normalized by the G-band. The spectra are offset for clarity.

The TGA curves recorded for as-received and treated CNTs are shown in Figure 6. Samples with a high amount of structural defects and/or amorphous carbon, i.e. higher I_D/I_G ratio, would be expected to present a lower temperature of combustion than samples with high purity and pristine walls. This is because structural defects and amorphous carbon are more reactive towards oxygen than carbon atoms forming the honeycomb graphene structure of the CNT walls. Indeed, steam treated SWCNTs present the lowest I_D/I_G ratio and the highest onset of combustion (580 ºC) whereas

sulfuric/nitric acid treated SWCNTs show the highest I_D/I_G ratio and the lowest onset of combustion (500 °C). Actually, the mixture of H_2SO_4/HNO_3 (3:1) is one of the most commonly used oxidants to introduce oxygen-bearing moieties on the surface of CNTs.[54] The TGA curve of this sample is characterized by three different weight losses. The first weight loss at ca. 100 °C corresponds to the evaporation of absorbed molecules (including water), which is followed with a continuous weight loss attributed to the removal of oxygen functionalities that leads to the complete combustion of the sample at 600 °C (this last process starts at ca. 500 °C). Piranha treated SWCNTs also start to lose weight at lower temperatures than the rest of samples and presents an onset of combustion at 516 °C. The temperature of the onset of combustion increases from 516 ºC up to 575 ºC after the steam treatment, with the corresponding decrease of the I_D/I_G ratio. This indicates that the structure of the SWCNTs can be greatly improved by performing a subsequent steam treatment.

In the case of MWCNTs, the samples presenting the highest onset of combustion are those that have undergone a steam treatment, either alone (12 h steam) or combined after the nitric/sulfuric cutting step (1 h steam). This observation seems contradictory to Raman data since the highest I_D/I_G ratio is recorded for both of these materials. According to Raman a large amount of defects or amorphous carbon is present in the samples, which as mentioned should result in a higher reactivity towards oxygen during TGA, i.e. low onset of combustion. Previous analyses by HRTEM revealed that no major differences were observed on the structure of the CNT walls before and after the steam treatment, nor functional groups could be detected by XPS or elemental analysis[32]. It is also worth pointing out that in the case of MWCNTs only the outer wall gets functionalized. Therefore, even if some functional groups were present their contribution to the whole sample would still be smaller than when using SWCNTs. The end-opening and shortening of the nanotubes could contribute to the I_D/I_G ratio since when opened, CNTs exhibit a higher amount of C sp^3[32]. TGA reveals the lowest onset of combustion temperature for ball milled MWCNTs at 373 °C. Several works have reported on the structural modification[55] and introduction of oxygen-containing functional groups by ball milling CNTs[56, 57] which might be at the origin of such low onset of combustion. H_2SO_4/HNO_3 treatment is

well known to introduce functionalities and as a consequence the sample is oxidized faster than the as-received material. The TGA curve of piranha treated MWCNTs is similar to that of as-received MWCNTs. This is in agreement with the statistical analysis performed above, which revealed no significant differences in their length distribution.

It is worth stressing that the combined protocol proposed herein (red TGA curves, Fig. 6), for SWCNTS (piranha + steam 1 h + HCl) and for MWCNTs (H_2SO_4/HNO_3 + steam 1 h + HCl) presents a higher onset of combustion temperature than the as-received CNTs (black TGA curve, Fig. 6). This indicates the removal of amorphous carbon and the most defective CNTs from the samples and the presence of a low amount of functional groups. The results of additional TGA measurements under flowing nitrogen are in agreement with this conclusion (Fig. S7). Both SWCNTs and MWCNTs cut by the combined treatment present a high thermal stability in an inert atmosphere, indicating the presence of minimal amounts of functional groups. Silva et al. have recently reported that steam treated CNTs are of such purity and crystallinity, that their oxidation temperature is closer to that of pristine graphene[58].

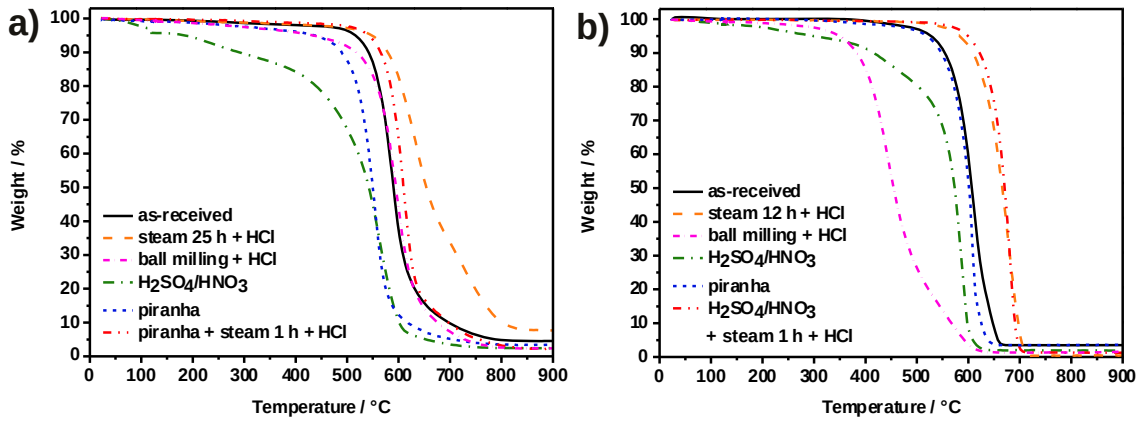

Figure 6. TGA of as-received and treated CVD CNTs with different methods: a) SWCNTs, b) MWCNTs. Measurements were performed under flowing air with a heating rate of 10 °C/min up to 900 °C.

The amount of residue collected after the complete combustion of CNTs corresponds to the amount of inorganic impurities present in the samples in their oxidized form. As-received SWCNTs

contained a 4.6 wt. % of inorganic material after TGA in air. The amount of inorganic impurities determined by TGA increases after the steam treatment (25 h steam + HCl) and decreases when employing any of the other treatments, in the range of 2.4-3.5 wt %. The increase of inorganic solid residue upon steam (and HCl) treatment has been previously observed. It does not mean that additional impurities are introduced during the processing but rather that the continous consumption of carbon from the sample results in an apparent increase of the amount of inorganic impurities [59]. Interestingly, the lowest inorganic content is achieved when employing the suggested combined protocol of piranha and steam (2.2 wt%).

The complete combustion of as-received MWCNTs leads to 3.5 wt. % of inorganic impurities. These can be efficiently decreased by any of the employed shortening/cutting strategies (down to 0.5-1.9 wt.%) but with the piranha treatment, which has no significant effect. The suggested combination of sulfuric/nitric acid followed by steam results in a 1.3 wt.% of inorganic impurities, after the complete oxidation of the sample. Taking into account that for instance iron nanoparticles, employed as catalyst for the growth of CNTs, would be oxidized to iron oxide after TGA, a smaller content of inorganic impurities is actually present in the sample of short CNTs. For instance if we consider that the collected solid residue arises only from iron present in the sample, 1.3 wt.% of iron oxide (Fe_2O_3) would actually correspond to 0.9 wt. % of Fe. Actually, silica and alumina have been detected in samples of as-received CNTs[32, 37]. Therefore, silica or alumina together with iron (from the catalyst) will contribute to the inorganic solid residue remaining after TGA in air. In order to evaluate the iron content in the samples, magnetization measurements were performed using a superconducting quantum interference device (SQUID). The iron content determined by SQUID has been included in Table 1, which summarizes the main characteristics of as-received and treated CNT samples. As it can be seen, a decrease in the iron content is observed for the suggested cutting strategies, from 1.4 wt. % to 0.9 wt. % when using the combined piranha and steam treatments for SWCNTs and from 1.5 wt.% down to 0.01 wt. % for the sulfuric/nitric acids and steam in the case of MWCNTs. The presence of high amounts of iron (ca. 40 wt. %) have been reported to contribute to CNTs' toxicity, because it acts as a catalyst for oxidative stress

[60, 61]. Although the levels of iron do not present a major concern for their use in the biomedical field for any of the investigated samples, the presence of catalytic impurities can dominate the electrochemical response of the material and cannot be overlooked [62].

XPS analysis was next performed on as-received CNTs on the samples obtained after using the proposed combined protocols to achieve of short CNTs. Analysis of the C1s high resolution spectra allows the detection of different functional groups [63]. For instance, oxygen-bearing functionalities that could have been introduced during the processing would be observed at binding energies below 290 eV. In the present case, no difference can be observed between the XPS curve of as-received CNTs and the processed material. According to previous analyses, as-produced Elicarb$^{(R)}$ CVD SWCNTs and MWCNTs do not present functional moieties on their backbone structure [32, 59]. Therefore, from the analyses performed so far we can conclude that no detectable functional groups are present after the proposed combined strategies to achieve samples of short CNTs.

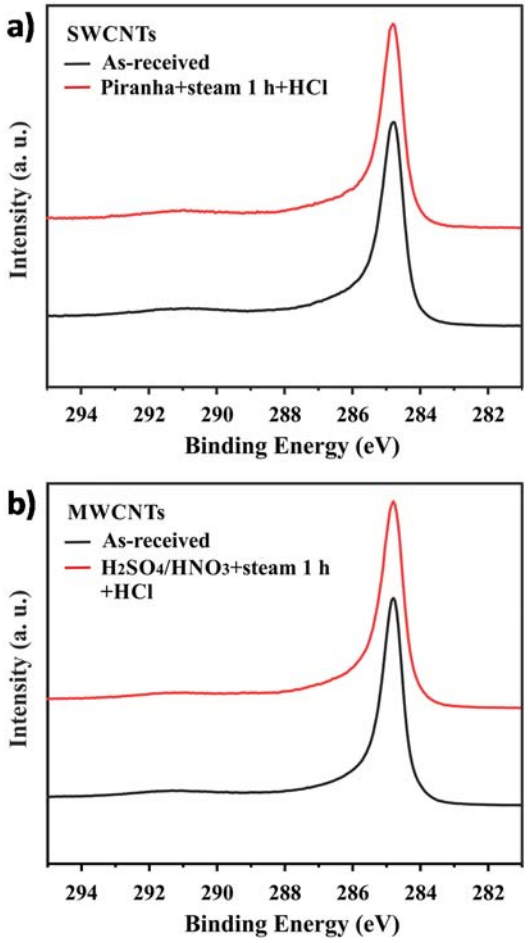

Figure 7. XPS spectra on the C 1s region of as-received CVD CNTs and after the optimized shortening treatment for a) SWCNTs and b) MWCNTs. Spectra have been normalized for an ease of comparison.

As mentioned in the introduction, the physico-chemical properties of carbon nanotubes are largely dependent on the source of the material (method employed for their synthesis). Therefore to complete the study, we investigated to which extend it was possible to achieve similar shortening/cutting degrees and length distributions when using CNTs from a different source. For this purpose, arc-discharged MWCNTs were independently treated by liquid phase (nitric/sulfuric) and gas phase (steam) reactions following exactly the same protocols employed for CVD grown MWCNTs. The length distribution of as-received and treated CNTs was determined by analysis of at least 200 individual CNTs by SEM. The resulting histograms are presented in Figure 8 and the fraction of arc-discharged MWCNTs with lengths below 500 nm in Figure S8. Visual inspection of the histograms already reveals that both strategies have reduced the lenght of arc-discharged MWCNTs.

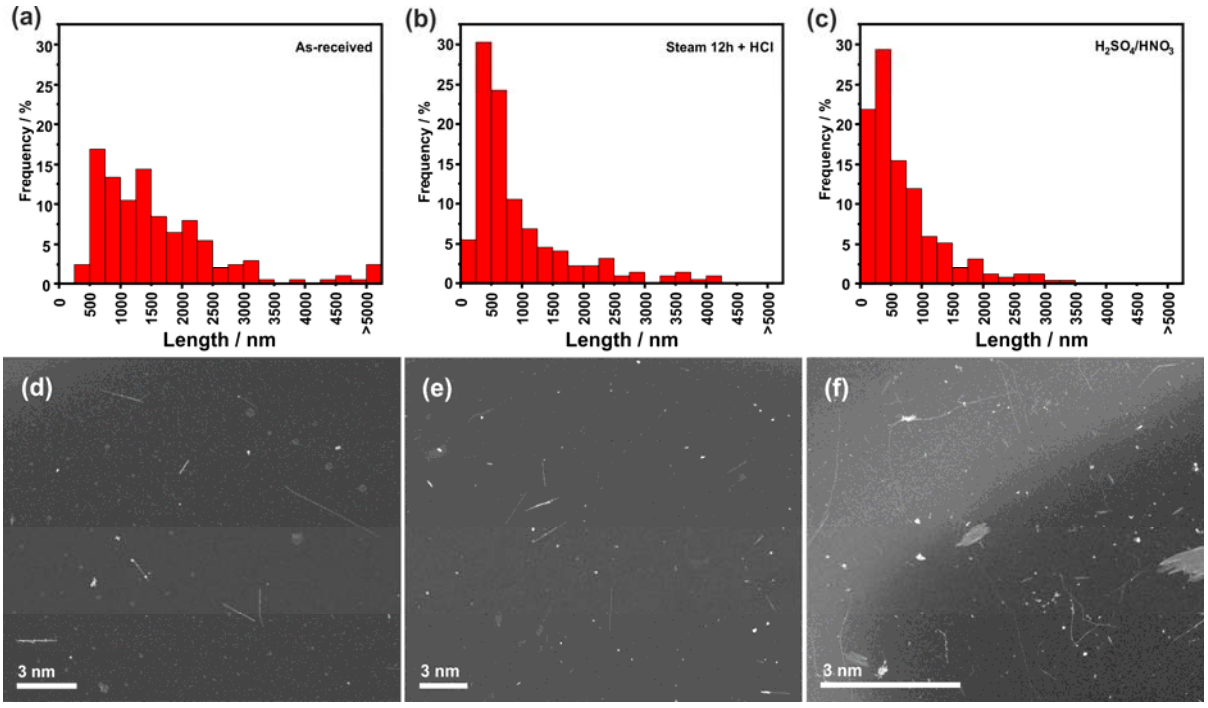

Figure 8. Length distribution histograms of (a) as-received, (b) steam 12h + HCl and (c) H_2SO_4/HNO_3 arc-discharged MWCNTs based on SEM image analysis. Representative SEM images employed to

determine the lenght distribution of MWCNTs are shown in (d) as-received, (e) steam 12h + HCl and and (f) H_2SO_4/HNO_3.

Table 2. Descriptive analysis of the length distribution for as-received and treated CVD and arc-discharged CNTs. At least 200 CNTs were measured for each sample.

MWCNTs	Faction below 500 nm (%)	Median (nm)	Lower adjacent observation (nm)	Q1 (nm)	Q3 (nm)	Maximum adjacent observation (nm)	Maximum observation (nm)
Arc-discharge							
as-received	3	1356	374	858	2032	3437	11909
steam 12 h + HCl	36	632	149	410	1173	2294	4176
H_2SO_4/HNO_3	51	495	115	274	926	1874	3397
CVD							
as-received	39	708	27	330	1469	3172	10084
steam 12 h + HCl	78	274	35	145	470	924	1899
H_2SO_4/HNO_3	68	365	31	183	611	1249	1779

Q1 - 25th percentile, Q3 - 75th percentile, IQR - interquartile range

For ease of comparison Table 2 presents the descriptive analysis of the length distribution for as-received, steam and nitric/sulfuric acid treated MWCNTs produced by CVD and arc-discharged. Note that the data for CVD MWCNTs was already included in Table 1 and Table S1. As it can be seen samples containing much shorter CNTs are obtained when using CVD MWCNTs than when employing arc-discharged MWCNTs using exactly the same treatments. The median lengths after steam + HCl turned out to be 274 nm (CVD) and 632 nm (arc-discharged), and after the nitric/sulfuric treatment 365 nm (CVD) and 495 nm (arc-discharged). Several factors can influence on the final length distribution of CNT samples such as the initial length of the as-received CNTs, the diameter of the CNTs and structural defects which in turn will affect their morphology.

Furthermore, whereas nitric/sulfuric is more efficient to reduce the length of arc-discharged MWCNTs (51 % below 500 nm) than steam (36 % below 500nm), the opposite seems to occur when using CVD MWCNTs (68 % below 500 nm for nitric/sulfuric and 78 % for steam). Steam has been reported to react through the ends of CNTs. As a consequence, longer reaction times would be needed to efficiently shorten arc-discharge MWCNTs (1356 nm median length, as-received) than the 12 h employed with CVD MWCNTs (708 nm median length, as-received).

From this comparative analysis, it becomes clear that the efficiency of a given method and the final lengths reported for CVD MWCNTs in this study can not be directly extrapolated to other types of CNTs. If short CNTs of a given length are needed for a given application, the experimental conditions will need to be adjusted to fulfill the requirement. CVD MWCNTs were employed in for the comparative study reported herein because CVD grown MWCNTs are the most commercially available source of CNTs nowadays.

4. Conclusions

We have shown that the source of CNTs might have an impact on the final length distribution of the CNTs after applying a given shortening/cutting strategy. Several commonly used shortening and cutting protocols have been employed onto a single batch of SWCNTs and another one of MWCNTs grown by CVD. These include chemical (steam, nitric/sulfuric acids and piranha) and physical methods (ball milling). Among the chemical methods, both gas phase (water steam) and liquid phase reactions (nitric/sulfuric, piranha) have been investigated. After each of the treatments, CNTs have been analyzed by SEM, Raman, SQUID and TGA to assess their length distribution, structure and purity. We have shown that SEM is as precise as AFM to determine the length of individual CNTs. Piranha cutting arises as a good approach to prepare short SWCNTs with a narrow length distribution in a good yield. In the case of MWCNTs the mixture of sulfuric/nitric acids turned out to be the most efficient in achieving a sample of short CNTs in a good yield. A subsequent 1 h steam treatment is suggested after processing the samples with either piranha (SWCNTs) or sulfuric/nitric acids (MWCNTs) to remove functionalities

from the sample, which is reflected in a higher thermal stability of CNTs and XPS data. The median length after the proposed combined treatments is 266 nm for CVD SWCNTs (piranha-steam) and 225 nm for CVD MWCNTs (sulfuric/nitric). Short CNTs are of interest for a broad range of applications, including biomedicine, electronics, water purification and composite materials.

Acknowledgements

The research leading to these results has received funding from the People Programme (Marie Curie Actions) of the European Union's Seventh Framework Programme FP7/2007-2013/ under REA grant agreement n°290023 (RADDEL). We acknowledge financial support from Spanish Ministry of Economy and Competitiveness through the "Severo Ochoa" Programme for Centres of Excellence in R&D (SEV-2015-0496, ICMAB; SEV-2013-0295, ICN2), and CHALENG (MAT2014-53500-R). M. K. also acknowledges support from the project LL1301 (MEYS). The ICN2 is funded by the CERCA programme (Generalitat de Catalunya). G. G. gratefully acknowledges the funding by European Commission under individual fellowship Marie Sklodowska-Curie (NANOTER, Grant Agreement 708351).We are thankful to Guillaume Sauthier from ICN2 for the XPS measurements. The authors would like to thank Thomas Swan Co. Ltd. for providing Elicarb© carbon nanotubes used for this study.

References

[1] Nie C, Galibert A-M, Soula B, Flahaut E, Sloan J, Monthioux M. A new insight on the mechanisms of filling closed carbon nanotubes with molten metal iodides. Carbon 2016;110:48-50.

[2] Ge H, Riss PJ, Mirabello V, Calatayud DG, Flower SE, Arrowsmith RL, et al. Behavior of Supramolecular Assemblies of Radiometal-Filled and Fluorescent Carbon Nanocapsules In Vitro and In Vivo. Chem 2017;3:437-60.

[3] Sandoval S, Pach E, Ballesteros B, Tobias G. Encapsulation of two-dimensional materials inside carbon nanotubes: Towards an enhanced synthesis of single-layered metal halides. Carbon 2017;123:129-34.

[4] Battigelli A, Ménard-Moyon C, Da Ros T, Prato M, Bianco A. Endowing carbon nanotubes with biological and biomedical properties by chemical modifications. Adv Drug Deliv Rev 2013;65:1899-920.

[5] Chen H, Zeng S, Chen M, Zhang Y, Li Q. Fabrication and functionalization of carbon nanotube films for high-performance flexible supercapacitors. Carbon 2015;92:271-96.

[6] Martin N, Da Ros T, Nierengarten J-F. Carbon nanostructures in biology and medicine. J Mater Chem B 2017;5:6425-7.

[7] Pascu SI, Arrowsmith RL, Bayly SR, Brayshaw S, Hu Z. Towards nanomedicines: Design protocols to assemble, visualize and test carbon nanotube probes for multi-modality biomedical imaging. Philos Trans R Soc A-Math Phys Eng Sci 2010;368:3683-712.

[8] Sun L, Wang X, Wang Y, Zhang Q. Roles of carbon nanotubes in novel energy storage devices. Carbon 2017;122:462-74.

[9] Kolanowska A, Janas D, Herman AP, Jędrysiak RG, Giżewski T, Boncel S. From blackness to invisibility – Carbon nanotubes role in the attenuation of and shielding from radio waves for stealth technology. Carbon 2018;126:31-52.

[10] Ali-Boucetta H, Nunes A, Sainz R, Herrero MA, Tian B, Prato M, et al. Asbestos-like Pathogenicity of Long Carbon Nanotubes Alleviated by Chemical Functionalization. Angew Chem Int Ed 2013;52:2274-8.

[11] Neves V, Heister E, Costa S, Tîlmaciu C, Flahaut E, Soula B, et al. Design of double-walled carbon nanotubes for biomedical applications. Nanotechnology 2012;23:365102.

[12] Smart SK, Cassady AI, Lu GQ, Martin DJ. The biocompatibility of carbon nanotubes. Carbon 2006;44:1034-47.

[13] Kolosnjaj-Tabi J, Hartman KB, Boudjemaa S, Ananta JS, Morgant G, Szwarc H, et al. In Vivo Behavior of Large Doses of Ultrashort and Full-Length Single-Walled Carbon Nanotubes after Oral and Intraperitoneal Administration to Swiss Mice. ACS Nano 2010;4:1481-92.

[14] Muller J, Huaux F, Moreau N, Misson P, Heilier J-F, Delos M, et al. Respiratory toxicity of multi-wall carbon nanotubes. Toxicol Appl Pharm 2005;207:221-31.

[15] Modugno G, Ksar F, Battigelli A, Russier J, Lonchambon P, Eleto da Silva E, et al. A comparative study on the enzymatic biodegradability of covalently functionalized double- and multi-walled carbon nanotubes. Carbon 2016;100:367-74.

[16] Dutt M, Nayhouse M, Kuksenok O, Little S, Balazs A. Interactions of End-functionalized Nanotubes with Lipid Vesicles: Spontaneous Insertion and Nanotube Self-Organization. Curr Nanosci 2011;7:699-715.

[17] Geng J, Kim K, Zhang J, Escalada A, Tunuguntla R, Comolli LR, et al. Stochastic transport through carbon nanotubes in lipid bilayers and live cell membranes. Nature 2014;514:612-5.

[18] Cabana L, Bourgognon M, Wang JTW, Protti A, Klippstein R, de Rosales RTM, et al. The Shortening of MWNT-SPION Hybrids by Steam Treatment Improves Their Magnetic Resonance Imaging Properties In Vitro and In Vivo. Small 2016;12:2893-905.

[19] Tan MLP. Long Channel Carbon Nanotube as an Alternative to Nanoscale Silicon Channels in Scaled MOSFETs. J Nanomat 2013;2013:5.

[20] Ma M, Grey F, Shen L, Urbakh M, Wu S, Liu JZ, et al. Water transport inside carbon nanotubes mediated by phonon-induced oscillating friction. Nat Nano 2015;10:692-5.

[21] Luan B, Zhou B, Huynh T, Zhou R. Controlled transport of DNA through a Y-shaped carbon nanotube in a solid membrane. Nanoscale 2014;6:11479-83.

[22] Liu H, He J, Tang J, Liu H, Pang P, Cao D, et al. Translocation of Single-Stranded DNA Through Single-Walled Carbon Nanotubes. Science 2010;327:64-7.

[23] Zhang L, Zhao B, Jiang C, Yang J, Zheng G. Preparation and Transport Performances of High-Density, Aligned Carbon Nanotube Membranes. Nanoscale Res Lett 2015;10:970.

[24] Das R, Ali ME, Hamid SBA, Ramakrishna S, Chowdhury ZZ. Carbon nanotube membranes for water purification: A bright future in water desalination. Desalination 2014;336:97-109.

[25] Sears K, Dumee L, Schuetz J, She M, Huynh C, Dumée L, et al. Recent Developments in Carbon Nanotube Membranes for Water Purification and Gas Separation. Materials 2010;3:127-49.

[26] Javey A, Guo J, Paulsson M, Wang Q, Mann D, Lundstrom M, et al. High-Field Quasiballistic Transport in Short Carbon Nanotubes. Phys Rev Lett 2004;92:106804.

[27] Cooper CA, Ravich D, Lips D, Mayer J, Wagner HD. Distribution and alignment of carbon nanotubes and nanofibrils in a polymer matrix. Compos Sci Technol 2002;62:1105-12.

[28] Fonseca A, Reijerkerk S, Potreck J, Nijmeijer K, Mekhalif Z, Delhalle J. Very short functionalized carbon nanotubes for membrane applications. Desalination 2010;250:1150-4.

[29] Liu J, Rinzler AG, Dai HJ, Hafner JH, Bradley RK, Boul PJ, et al. Fullerene Pipes. Science 1998;280:1253-6.

[30] Gu Z, Peng H, Hauge RH, Smalley RE, Margrave JL. Cutting Single-Wall Carbon Nanotubes through Fluorination. Nano Lett 2002;2:1009-13.

[31] Chen ZY, Hauge RH, Smalley RE. Ozonolysis of Functionalized single-Walled Carbon Nanotubes. J Nanosci Nanotechnol 2006;6:1935-8.

[32] Cabana L, Ke X, Kepić D, Oro-Solé J, Tobías-Rossell E, Van Tendeloo G, et al. The role of steam treatment on the structure, purity and length distribution of multi-walled carbon nanotubes. Carbon 2015;93:1059-67.

[33] Banhart F, Li J, Terrones M. Cutting Single-Walled Carbon Nanotubes with an Electron Beam: Evidence for Atom Migration Inside Nanotubes. Small 2005;1:953-6.

[34] Jung C-H, Kim D-K, Choi J-H, Nho Y-C, Shin K. Shortening of multi-walled carbon nanotubes by gamma-irradiation in the presence of hydrogen peroxide. Nucl Instrum Methods Phys Res B 2008;266:3491-4.

[35] Zhou J, Cheiftz J, Li R, Wang F, Zhou X, Sham T-K, et al. Tailoring multi-wall carbon nanotubes for smaller nanostructures. Carbon 2009;47:829-38.

[36] Rubio N, Fabbro C, Herrero MA, de la Hoz A, Meneghetti M, Fierro JLG, et al. Ball-Milling Modification of Single-Walled Carbon Nanotubes: Purification, Cutting, and Functionalization. Small 2011;7:665-74.

[37] Kierkowicz M, Pach E, Santidrián A, Tobías-Rossell E, Kalbáč M, Ballesteros B, et al. Effect of Steam-Treatment Time on the Length and Structure of Single-Walled and Double-Walled Carbon Nanotubes. ChemNanoMat 2016;2:108-16.

[38] Lim JK, Yun WS, Yoon M-h, Lee SK, Kim CH, Kim K, et al. Selective thiolation of single-walled carbon nanotubes. Synth Met 2003;139:521-7.

[39] Ziegler KJ, Gu ZN, Shaver J, Chen ZY, Flor EL, Schmidt DJ, et al. Cutting single-walled carbon nanotubes. Nanotechnology 2005;16:S539-S44.

[40] Tobias G, Shao L, Salzmann CG, Huh Y, Green MLH. Purification and Opening of Carbon Nanotubes Using Steam. J Phys Chem B 2006;110:22318-22.

[41] Li YB, Wei BQ, Liang J, Yu Q, Wu DH. Transformation of carbon nanotubes to nanoparticles by ball milling process. Carbon 1999;37:493-7.

[42] Liu J, Rinzler AG, Dai H, Hafner JH, Bradley RK, Boul PJ, et al. Fullerene Pipes. Science 1998;280:1253-6.

[43] Lange A, Brauer H-D. On the formation of dioxiranes and of singlet oxygen by the ketone-catalysed decomposition of Caro's acid. J Chem Soc, Perkin Trans 2 1996:805-11.

[44] Edwards HGM, Turner JMC, Fawcett V. Raman spectroscopic study of nitronium ion formation in mixtures of nitric acid, sulfuric acid and water. J Chem Soc, Faraday Trans 1995;91:1439-43.

[45] Lin C-C, T. T. Chu B, Tobias G, Sahakalkan S, Roth S, L. H. Green M, et al. Electron transport behavior of individual zinc oxide coated single-walled carbon nanotubes. Nanotechnology 2009;20:105703.

[46] Bortolamiol T, Lukanov P, Galibert A-M, Soula B, Lonchambon P, Datas L, et al. Double-walled carbon nanotubes: Quantitative purification assessment, balance between purification and degradation and solution filling as an evidence of opening. Carbon 2014;78:79-90.

[47] Reich S. TC, Maultzsch J. Carbon Nanotubes: Basic Concepts and Physical Properties: John Wiley & Sons 2004.

[48] Dresselhaus MS, Dresselhaus G, Jorio A, Souza Filho AG, Saito R. Raman spectroscopy on isolated single wall carbon nanotubes. Carbon 2002;40:2043-61.

[49] Jorio A, Souza AG, Dresselhaus G, Souza-Filho AG, Dresselhaus MS, Swan AK, et al. G-band resonant Raman study of 62 isolated single-wall carbon nanotubes. Phys Rev B 2002;65.

[50] Pimenta MA, Marucci A, Empedocles SA, Bawendi MG, Hanlon EB, Rao AM, et al. Raman modes of metallic carbon nanotubes. Phys Rev B 1998;58:R16016-R9.

[51] Pimenta MA, Hanlon EB, Marucci A, Corio P, Brown SDM, Empedocles SA, et al. The anomalous dispersion of the disorder-induced and the second-order Raman Bands in Carbon Nanotubes. Braz J Phys 2000;30:423-7.

[52] Salzmann CG, Llewellyn SA, Tobias G, Ward MAH, Huh Y, Green MLH. The Role of Carboxylated Carbonaceous Fragments in the Functionalization and Spectroscopy of a Single-Walled Carbon-Nanotube Material. Adv Mater 2007;19:883-7.

[53] Kang CS, Lee IJ, Seo MS, Kim SH, Baik DH. Effect of purification method on the electrical properties of the carbon nanotube fibers. Fiber Polym 2017;18:1580-5.

[54] Datsyuk V, Kalyva M, Papagelis K, Parthenios J, Tasis D, Siokou A, et al. Chemical oxidation of multiwalled carbon nanotubes. Carbon 2008;46:833-40.

[55] Ahn JH, Shin HS, Kim YJ, Chung H. Structural modification of carbon nanotubes by various ball milling. J Alloy Compd 2007;434-435:428-32.

[56] S.K. Smart, W.C. Ren, H.M. Cheng, G.Q. Lu, Martin DJ. Shortened double-walled carbon nanotubes by high-energy ball milling. Int J Nanotech 2007;4:618-33.

[57] Park KC, Fujishige M, Takeuchi K, Arai S, Morimoto S, Endo M. Inter-collisional cutting of multi-walled carbon nanotubes by high-speed agitation. J Phys Chem Solids 2008;69:2481-6.

[58] King SG, McCafferty L, Stolojan V, Silva SRP. Highly aligned arrays of super resilient carbon nanotubes by steam purification. Carbon 2015;84:130-7.

[59] Ballesteros B, Tobias G, Shao L, Pellicer E, Nogués J, Mendoza E, et al. Steam Purification for the Removal of Graphitic Shells Coating Catalytic Particles and the Shortening of Single-Walled Carbon Nanotubes. Small 2008;4:1501-6.

[60] Kagan VE, Tyurina YY, Tyurin VA, Konduru NV, Potapovich AI, Osipov AN, et al. Direct and indirect effects of single walled carbon nanotubes on RAW 264.7 macrophages: Role of iron. Toxicol Lett 2006;165:88-100.

[61] Pulskamp K, Diabaté S, Krug HF. Carbon nanotubes show no sign of acute toxicity but induce intracellular reactive oxygen species in dependence on contaminants. Toxicol Lett 2007;168:58-74.

[62] Pumera M, Miyahara Y. What amount of metallic impurities in carbon nanotubes is small enough not to dominate their redox properties? Nanoscale 2009;1:260-5.

[63] T.I.T. Okpalugo, P. Papakonstantinou, H. Murphy, J. McLaughlin, Brown NMD. High resolution XPS characterization of chemical functionalised MWCNTs and SWCNTs. Carbon 2005; 43: 153-161.